DYNAMICS OF PULSED HIGH CURRENT RELATIVISTIC ELECTRON BEAMS*

S. E. Graybill
Ion Physics Corporation
Burlington, Massachusetts

SUMMARY

Pulsed electron beams are formed by the slow charge of a pulse forming network (microseconds to D.C.) and the fast discharge (10 - 100 ns) onto a field emission diode. The resultant beams of kiloamps to megamps at hundreds of keV to ten MeV are passed through a window into the drift region. Ionization in the drift section allows the beam to be confined by its own magnetic field. Secondary electron currents in the plasma tend to neutralize this effect. Recent work on guiding intense beams with auxiliary fields has utilized applied B_z and B_θ (z-pinch) fields. Application of these beams extends from shock studies to ion acceleration.

INTRODUCTION

It is the intent of this paper to review the advances made in the field of high current relativistic electron beams. The field is approximately six years old although the first theoretical treatments were done much earlier.[1, 2, 3] Machines capable of delivering these beams were being developed in the early 1960's.[4] The first observation of these beams was reported by Graybill and Nablo in 1965.[5]

The beams of interest here are characterized by the following parameters:

Electron Energy	100 keV	-	10 MeV
Beam Current	10 kA	-	1 MA
Pulse Width	10 ns	-	100 ns
Energy Delivered	10 kJ	-	1 MJ

These beams are normally utilized with current densities in the 10^3 - 10^4 amps/cm^2 range so the electron densities are in the 10^{11} - 10^{12}/cm^3 range. Such particle densities are far greater than found in the beams from conventional particle accelerators but several orders of magnitude less than typical plasma densities. The drift region for these beams is generally filled with a gas to particle densities of 10^{15} - 10^{16}/cm^3. The degree of ionization of this background gas is apparently quite large.[6]

ACCELERATORS

A description of the many generators now operational is beyond the scope of this paper and can be found in many references.[7-14] All machines contain a pulse forming network which is a transmission line that is switched on to a field emission diode. The pulse forming line may be coaxial or biplanar[10] and is generally pulse charged, but can be d.c.[8, 13] charged. The line may be folded into the Blumlein configuration for voltage doubling.[7, 10, 11]

The dielectric may be high pressure gas,[8, 13] oil,[7, 11] water,[14] or mylar.[10]

The advantages and disadvantages of these many schemes constitute a large field of study that will not be discussed here.

FIELD EMISSION DIODE

The field emission diodes used in pulsed electron beam work are predominately of the type first designed at Aldermaston, England by J. C. Martin and co-workers.[4] Figure 1 shows the tube used on "Neptune" the Ion Physics water line machine. This figure serves to illustrate the basic design features of the diode. The dielectric spacers are angled on the vacuum side to enhance the voltage standoff[4] and are separated by metal planes. The tube is capacitively graded, which in the case of water dielectrics requires stress relieving rings (not shown). Cathodes range from rods with hemispherical ends for high impedance machines to large area emitters for low impedance applications. The low impedance cathodes may be multi-point, concentric circular edges, or epoxy filled metal honeycomb to name some of the commonly used emitters. The beam passes through a window which is thin mylar or kapton at low voltages and titanium at high voltages.

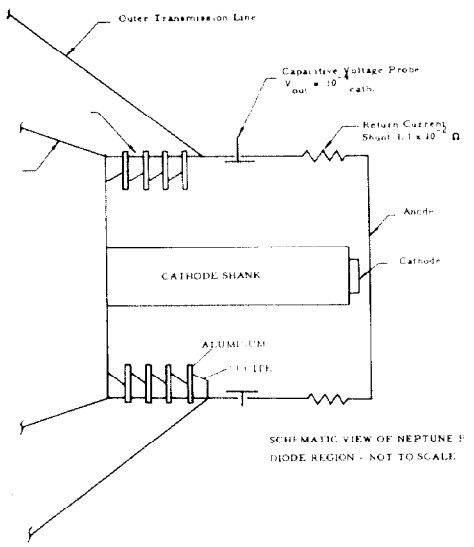

Figure 1. Schematic view of Neptune B diode region.

Although the mechanism for emission is not known in detail it is generally accepted now that a field emission initiated plasma at the cathode surface is the

*Work partially supported by the Defense Atomic Support Agency.

true emitter and all cathodes are space charge limited. In the limit of a high impedance cathode with a hemispherical tip, Boers[15] has shown that $Z \approx 30 \ln \frac{r_o}{r_c}$ where r_o is the radius of the cathode extension region and r_c is the tip radius. For low impedance cathodes of the planar type the upper limit of impedance is predicted by the non-relativistic Child-Langmuir space charge relation from which one obtains the expression

$$Z_{C-L} = \frac{136 \left(\frac{d}{r}\right)^2}{\sqrt{V}} ,$$

where V is in megavolts, d is the gap spacing and r is the cathode radius. Observed impedances are equal to or less than Z_{C-L},[10] possibly due to ions formed in the gap. This expression has been derived with the relativistic correction by Boers and Kelleher[35] and it is shown that the above relation is quite good up to a few MeV.

In Figure 1 the tube diagnostics used at Ion Physics are shown. These consist of a capacitive voltage divider and a return current shunt. The voltage monitor encircles the cathode shank in order to gain sensitivity (order of 100 V signal per megavolt on the shank). The return current shunt consists of a band of parallel low value resistors interrupting the return current path. The sensitivity of these diagnostics is measured in place by use of an applied long pulse and the rise time is measured in a bench test by making the unit part of a tapered biconic transmission line down which a subnanosecond rise square pulse is launched.

The outputs of these diagnostics are recorded on synchronized oscilloscopes and yield information typified by Figure 2, which shows data from one of the Ion Physics gas insulated machines. Here the voltage has been corrected for the inductive contribution due to the monitor being behind the cathode tip. The time dependent behavior of the gap imedance is typical and it is seen that the cathode plasma apparently takes about 10 ns to form as evidenced by the value of Z decreasing rapidly in that time and then becoming essentially constant. Figures 3a and 3b show the electron energy spectrum as obtained from the current-voltage waveforms and measured by a 180° magnetic spectrometer.

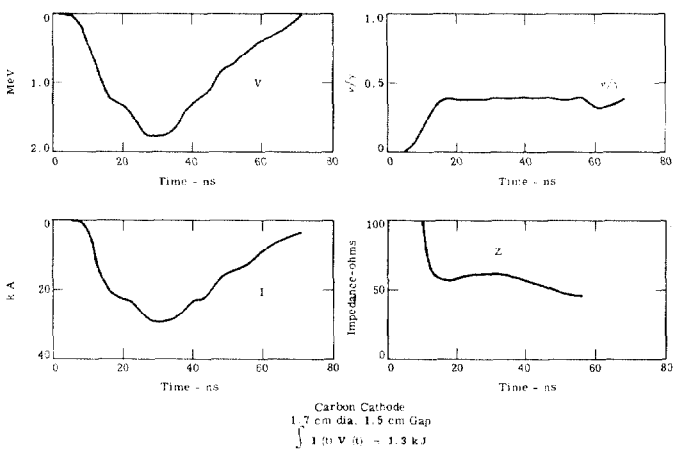

Figure 2. Field Emission Diode Characteristics.

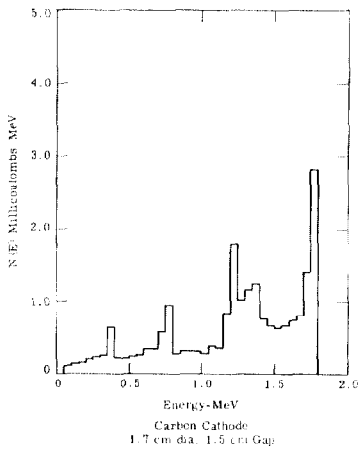

Figure 3a. Energy spectrum derived from current-voltage waveforms.

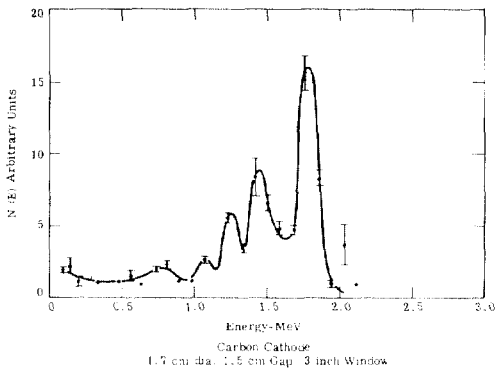

Figure 3b. Magnetically analyzed energy spectrum.

LAWSON THEORY

Lawson's basic analysis is useful in understanding electron beam motion although his assumptions are quite restrictive. Most important are the assumptions that $\frac{\beta_r}{\beta_z} \ll 1$ (Paraxial assumption), current density is uniform and the fractional ionization is uniform. Lawson's radial equation of motion accounting for the electric and magnetic forces on an electron in such a stream is

$$\frac{d^2 r}{dz^2} = 2\nu/\gamma \frac{r}{r_o^2} \frac{(1-f-\beta^2)}{\beta^2}$$

where $\nu = N_e r_e$. N_e is the number of electrons per unit length and r_e is the classical electron radius.

$$N_e = \frac{I}{e\beta c} , \quad r_e = \frac{e^2}{4\pi\epsilon_o mc^2}$$

$$\nu/\gamma = \frac{I}{\beta\gamma} \frac{e\mu_o}{4\pi mc} = \frac{I}{17{,}000\,\beta\gamma}$$

$$f = \frac{n_I}{n_e}$$

The first item to note is that for a beam to propagate in a confined mode we require

$$f > 1 - \beta^2 = \frac{1}{\gamma^2}$$

This degree of ionization is required for the magnetic pinching to overcome the electrostatic repulsion.

Assuming that f = 1, the wave length of the sinusoidal solution is

$$\lambda = \frac{2\pi r_o}{\sqrt{2\nu/\gamma}}$$

so that $2\nu/\gamma < 1$ or $I < 8500\beta\gamma$ amps is the criterion for the paraxial assumption to be valid.

Lawson and Alfven have also noted that since the radius of curvature of an electron at the edge of the beam

$$\rho = \frac{P}{eB} = \frac{m\gamma\beta c}{e} \quad \frac{2\pi r_b}{\mu_o I} \quad \text{so that}$$

$$\frac{r_b}{\rho} = \frac{e\mu_o}{2\pi mc} \quad \frac{I}{\beta\gamma} = 2\nu/\gamma = \frac{I}{8500\beta\gamma}$$

So if $I = 17,000\beta\gamma$ amps ($\nu/\gamma = 1$) the electron will, under this model, turn around. The same argument has been applied to the cathode anode gap where one demands that $\rho = \frac{r_b}{2\nu/\gamma} > d$, the gap spacing, so $\nu/\gamma < \frac{r_b}{2d}$ for the beam to not pinch in the diode.

BEAM PROPAGATION

The basic elements of beam propagation can be seen in the following description of a 1.5 MeV beam, $\nu/\gamma = 0.5$ which has been studied at Ion Physics. In Figure 4 are shown the results of a segmented calorimeter placed in the drift tube 20 cm from the beam entrance window. The beam is seen to focus as the ionization fraction grows due to the higher gas pressure up to .2 torr. Above .2 torr the fluence decreases reaching a minimum in the one torr region. This defocusing behavior was first explained by Link[7] and in more detail by Yonas and Spence[12] as due to plasma return currents being driven by the $\dot{B}$ forces at the head of the beam reducing the beam's own magnetic field. It will be seen that this pressure permits the most efficient transport of energy by the beam. As the pressure is increased above a few torr the plasma conductivity decreases due to the short mean free path available to the secondary electrons and the beam again pinches. This behavior is seen graphically in the open shutter photographs in Figure 5.

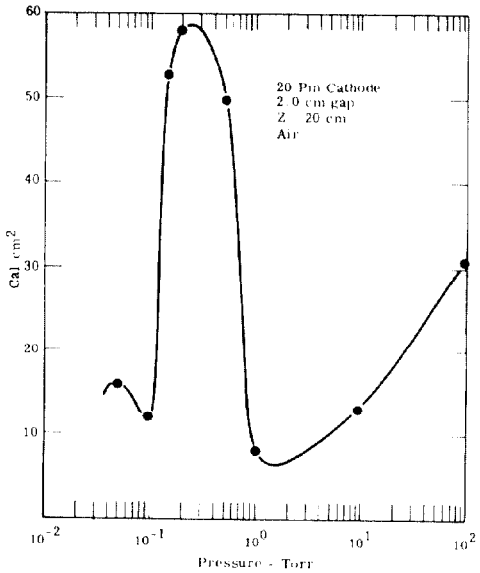

Figure 4. Beam energy fluence.

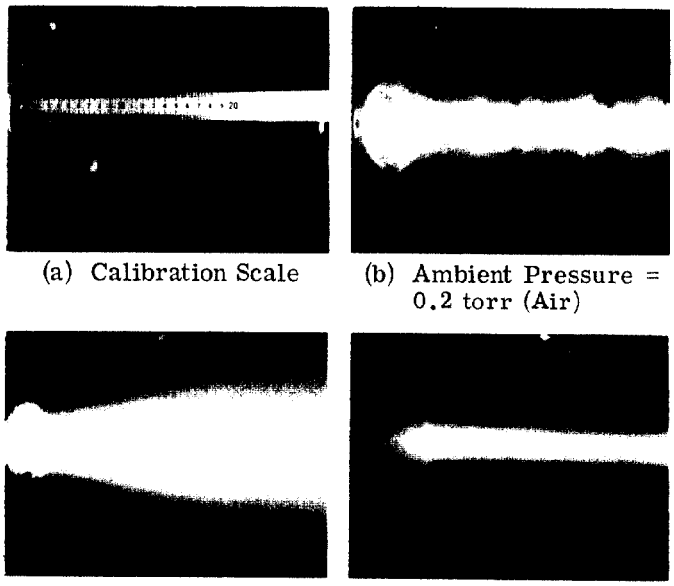

(a) Calibration Scale

(b) Ambient Pressure = 0.2 torr (Air)

(c) Ambient Pressure = 1.0 torr (Air)

(d) Ambient Pressure = 100.0 torr (Air)

Figure 5. Beam plasma photographs for a multi-point, low impedance cathode.

This theory is further confirmed by monitoring the return current flowing in the drift tube wall with resistive shunts as shown in Figure 6.

These shunts measure net current which is defined as the beam primary current plus the plasma secondary current. The results are shown in Figure 7 where the wall current versus pressure is plotted for three different times during the pulse. It is seen as expected that the net current is a minimum at one torr. It is approximately ten percent of the primary current.

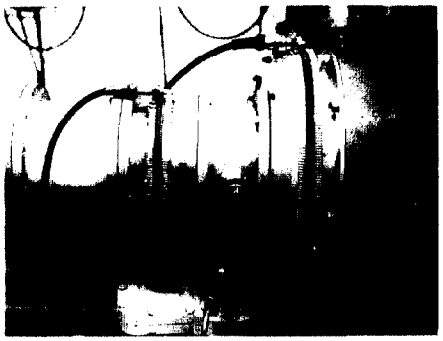

Figure 6. Drift tube and field emission tube current shunts.

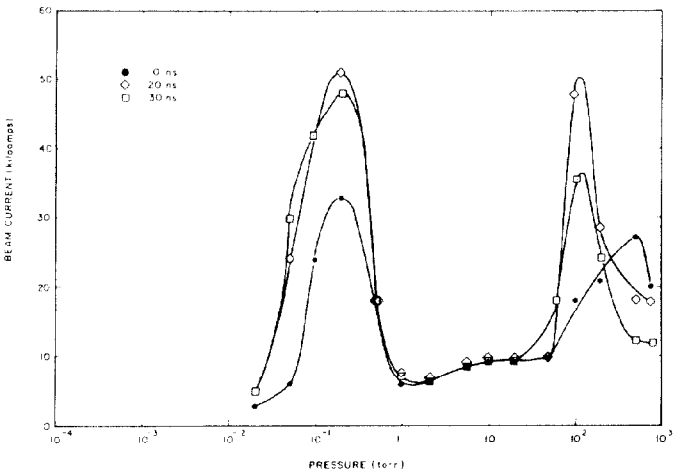

Figure 7. Wall current as a function of drift tube pressure (air).

The largest energy fluence was observed at high net current (high degree of focusing) as expected but the most efficient energy transport over significant distances occurs at minimum net current as shown in Figure 8.

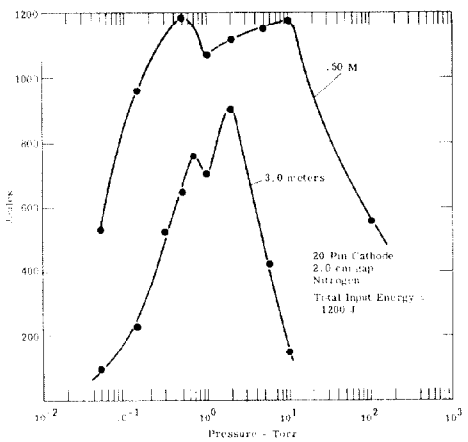

Figure 8. Total transmitted beam energy.

This plot shows the total transported energy at 0.5 and 3.0 meters as a function of pressure and demonstrates the importance to energy transport of minimizing the electron radial velocity (low net current).

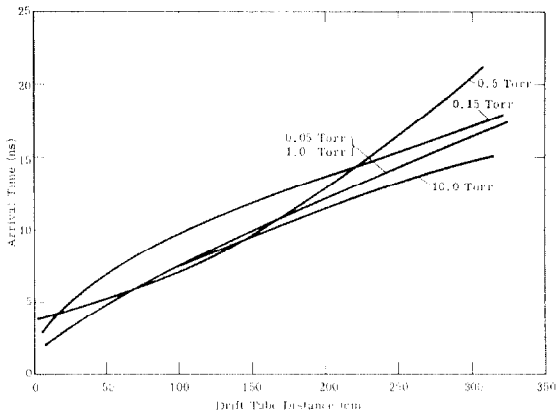

Figure 9. Electron beam arrival time versus distance 20 pin cathode, 2.0 cm. gap.

In Figure 9 we see that the maximum transit velocity of the beam front occurs at very low pressure where the current is low due to loss through space charge repulsion and at one to ten torr where the net current is minimum.

Studies of the propagation of high $\nu/\gamma \approx 10$ beams have been reported by Yonas and Spence[12] using a Physics International oil insulated pulser. They note that,

1. Beams only propagate over significant distances if

$$(\nu/\gamma)_{net} = \frac{\left[\vec{I}_{primary} + \vec{I}_{plasma}\right]}{17,000\,\beta\gamma} < 1$$

2. Gas breakdown in the electric field due to the rising magnetic field of the beam is the mechanism providing plasmas of sufficient conductivity to obtain the observed current neutralization.

3. Beam front velocity is less than that of the later parts of the beam due to beam front losses.

4. Beam front velocity is greatest at one torr (as we have observed at $\nu/\gamma = 0.5$).

5. Energy deposition measurements indicate $(\nu/\gamma)_{net} = 1$ based on Lawson's[16] relation

$$\frac{\langle \beta_r^2 \rangle}{\langle \beta_z^2 \rangle} \approx \nu/\gamma$$

Figure 10 (from Reference 12) shows net current current versus pressure, and breakdown and decay time versus pressure where breakdown time is the pulse rise time and decay time is that of the net current pulse. It is seen that the net current decreases with breakdown time as pressure increases and then increases with decreasing decay time above one torr. This model is consistent with the data that went into Figure 7.

Ion Physics data shows the e folding length for total beam energy transport to be 10 meters at

ν/γ = .5, 6 meters at ν/γ = 1.5-3 and Physics International shows the e folding distance to be 2 meters for ν/γ = 10. Also noting that current neutralization factors of greater than ten have not been observed one concludes that beams of $\nu/\gamma > 10$ will not propagate for significant distances. These facts coupled with the noting of beam front erosion due to space charge loss, retarding of the beam front from B fields, and loss from radial momentum components present at injection led researchers to aid beam transport with auxiliary fields.

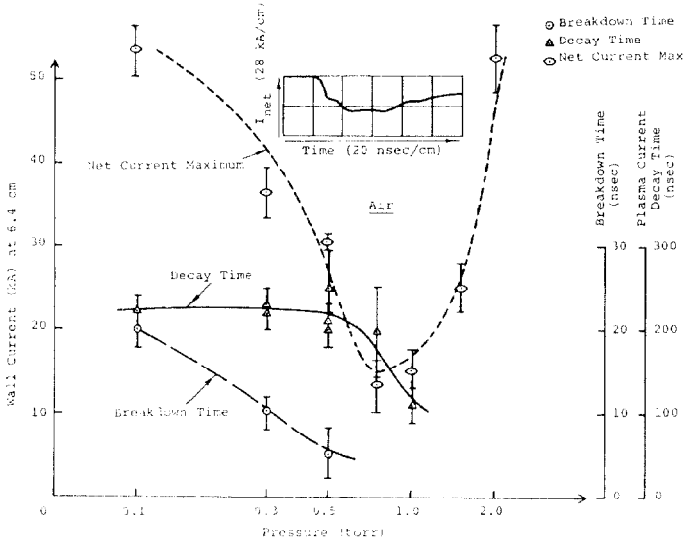

Figure 10. Net current, plasma current decay time, and breakdown time versus pressure in air.

LONGITUDINAL MAGNETIC FIELDS

The theory of magnetic guide fields on beams has been discussed in detail by Andrews et al[17] and their effect in preventing diode pinching by Hammer et al.[34] Recent work by Bzura and Linke[18] has shown the energy transport at 2.5 meters of a 400 keV, 60 kA beam in 0.5 torr to be increased from just over 60% to 90% with a 2 kG field as shown in Figure 11. Even more impressive is the data shown in Figure 12 where almost 80% transport is achieved at one meter without a metal return path (non-conductive drift tube).

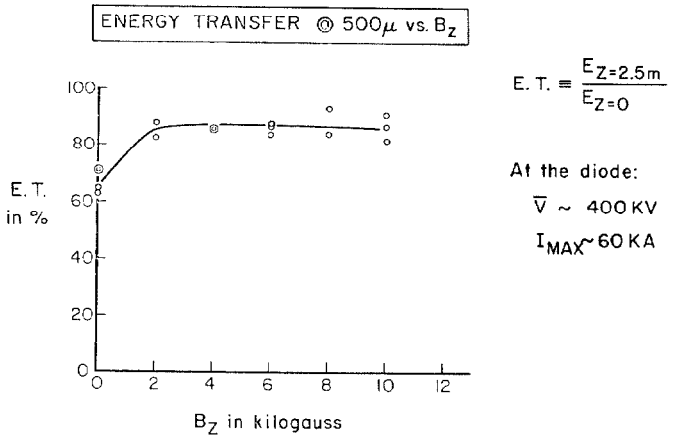

Figure 11. Energy transfer at 500 μ versus B_Z.

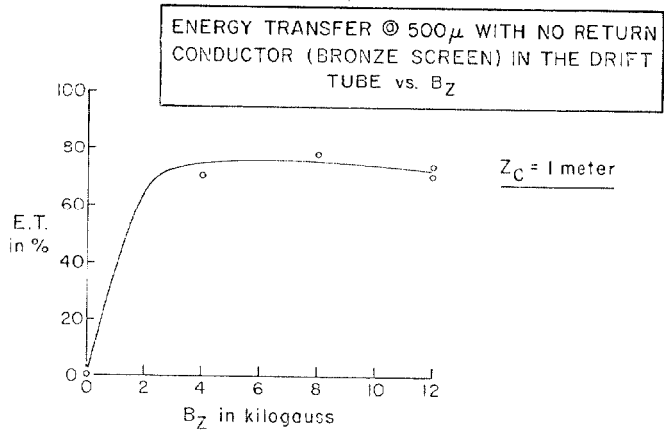

Figure 12. Energy transfer at 500 μ with no return conductor (bronze screen) in the drift tube versus B_Z.

Another intersting result is that of Friedman and Ury where a beam was extracted from the tube without a conventional window using a magnetic guide field.[19] In this experiment the electrons are guided from a biconic cathode-anode region into a drift region both at low pressure (~5 x 10^{-4} torr).

Z-PINCH CONFINEMENT

Benford and Ecker have reported the confinement of high ν/γ (=7) beams using $B\theta$ confinement[20] produced by a z-pinch. They find pinch currents much lower than the beam current will confine and propagate the beam. Figure 13 shows the radial distribution of $B\theta$ due to the z-pinch at different times during the pinch. The electron beam was then launched parallel and coaxial to the pinch current through a common electrode (the beam window). The confinement of the beam was ascertained by the damage patterns on targets at the far end of the pinch region. The damage radii at different pinch currents is shown in Figure 14.

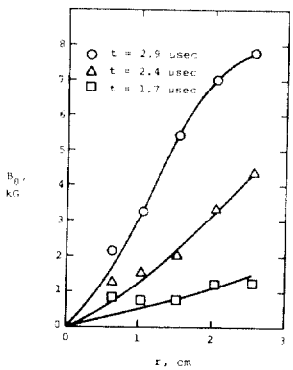

Figure 13. Azimuthal magnetic field profiles of z-pinch.

APPLICATION

The beams we have discussed have a wide variety of applications. They have been used for the study of material parameters, ion acceleration, Astron studies, plasma heating, and flash radiography.

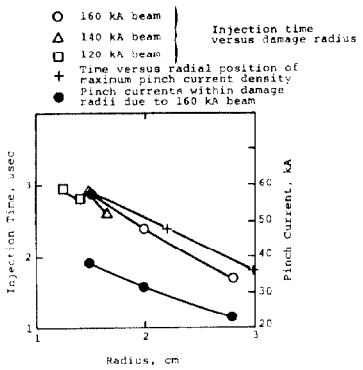

Figure 14. Damage radii, injection times, collapse trajectory of pinch current sheath, and amounts of pinch current inside damage radii of 160 kA beams.

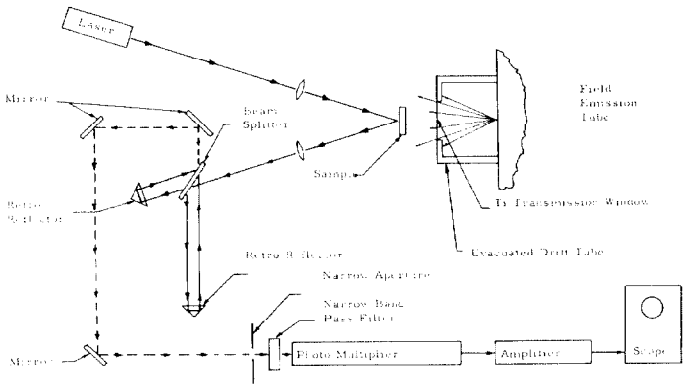

Figure 15. Experimental arrangement depicting velocity interferometer.

An application of these beams to materials studies is described by Oswald et al[21, 22] where a laser illuminated, Michelson interferometer is used to study the deflection of the rear surface of a sample when the front is pulsed with the electron beam. The shock is propagated through the sample causing the rear surface to deflect. The rear surface is one of the mirrors of the interferometer and when it moves the interference pattern shifts. By illuminating a slit in front of a photomultiplier tube with the interference pattern the illumination will change as fringes go past the slit. Thus an a.c. signal is produced by the P.M. tube and displayed on an oscilloscope. By calculating the energy deposition and observing the rear surface deflection relevant material parameters can be deduced. This technique is now being extended to measuring velocity directly with a velocity sensitive interferometer as shown in Figure 15.[23]

Another exciting recent use of these beams has been the experiment by Fleischmann[24] where the beam from the Cornell pulser[10] was trapped in a magnetic field with an Astron geometry. Field reversal was obtained and the containment time was several hundred nanoseconds.

Relevant to ERA application is the measurement of the emittance of the central portion of a field emission diode at Ion Physics Corporation.[25] The field emitted beam was passed through small holes in tantalum as shown in Figure 16 and the images recorded on blue cellophane dosimetry. A scan of the blue cellophane yielded data which produced the emittance diagrams shown in Figure 17.

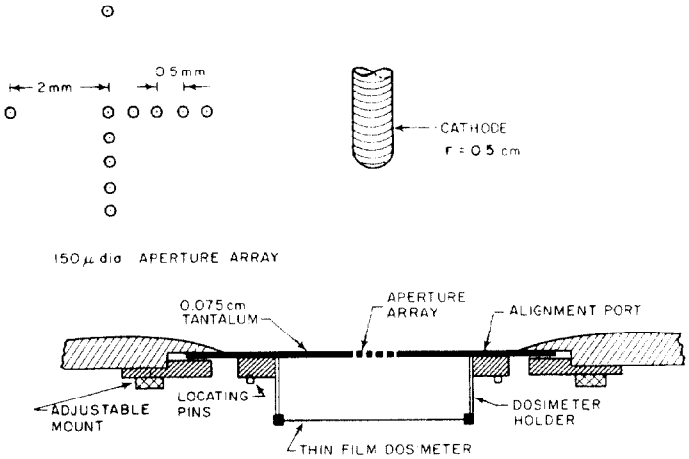

Figure 16. Emittance measurement configuration.

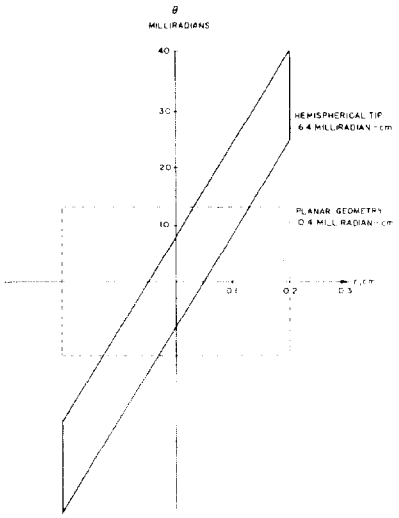

Figure 17. Emittance diagrams for planar and hemispherical emitters.

One of the more interesting applications of these beams is the acceleration of ions to energies higher than that of the electrons.[26-33] This phenomenon was first observed at Ion Physics[26] where time of flight measurements were made, and shortly after at Physics International where magnetic analyses coupled with nuclear emulsions were employed.[27]

Graybill and Uglum[30, 31] have improved upon their ion time of flight technique reported earlier and utilized a 1.7 MeV, 30 kA beam, a slightly higher impedance than that used previously. The results of these experiments are summarized in Figures 18 and 19. Two time references were checked, namely the leading edge of the ion current pulse and also the peak of the ion current pulse. There is a slight difference in the ion velocity versus pressure for the two ways of analyzing the data, but in general the results are consistent. Each data point represents the average value of arrival time of two or three separate measurements.

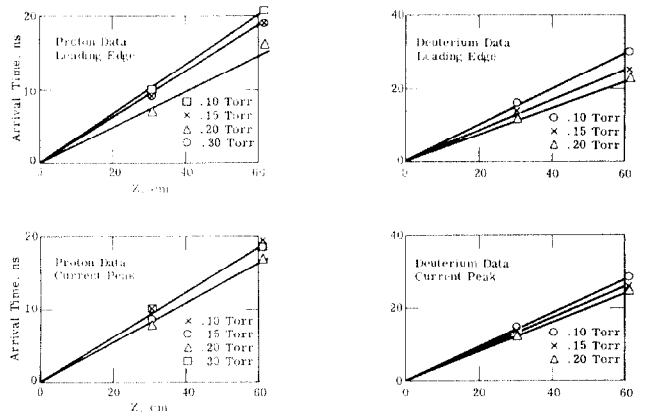

Figure 18. Ion time of flight - hydrogen and deuterium.

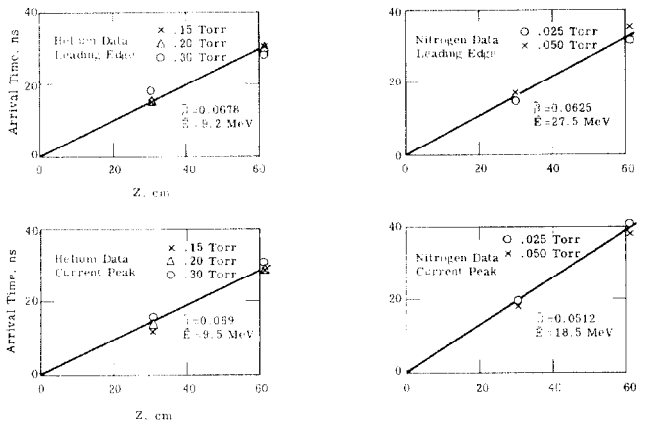

Figure 19. Ion time of flight - helium and nitrogen.

The results show that, for helium and nitrogen, the ion energy is not pressure dependent over the range of pressure studied, while hydrogen and deuterium do exhibit a dependence of ion energy on pressure. The plots shown in Figure 20 make this more apparent.

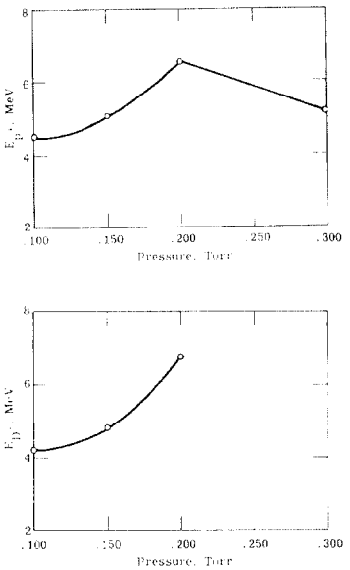

Figure 20. Pressure dependence of proton and deutron energies.

The energy and species observed were confirmed by doing range measurements in aluminum and a magnetic analysis.

The experimental results of the magnetic analysis are shown in Figure 21. The hydrogen data was used to calibrate the system. The arrows on the other plots show where the indicated species' charge state will occur given the hydrogen calibration and the velocity measurements. The deuterium and helium data prove that only the filling gas species is present, and for helium the indication is that only completely ionized atoms are accelerated. The nitrogen data shows that highly stripped ions are formed, with the main contribution coming from six-times ionized nitrogen.

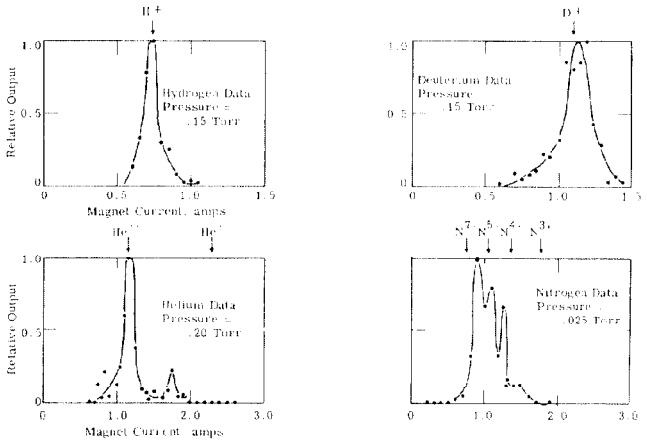

Figure 21. Magnetic analysis data for various ions.

The high ion currents available are shown in Figure 22 which shows the oscilloscope traces obtained from the current collector for various gases. The total currents range from 100 - 200 A of photons to ~10 A of nitrogen ions.

Measurements were made of the neutron yields obtainable from the accelerated ion beams using Be (x, n) reactions. Protons, deuterons, and helium ions were allowed to impinge on a beryllium plate located on the blank-off plate at the end of the main drift tube with the result that something approaching 10^{10} neutrons/pulse is obtained.

An experiment was carried out to determine the influence of drift tube length on the acceleration process in which the time of arrival of the ion pulse at the end of the drift tube was measured at different pressures and lengths. The results are shown in Figure 23.

It is seen from Figure 23 that the ions originate and are accelerated in the first thirty centimeters of the drift region. They also apparently originate about 10 nanoseconds after the electron current begins and it is also obvious that they travel much more slowly than the beam front.

Rander, Ecker and Yonas at Physics International have investigated this phenomenon with somewhat different results.[27,28,33] They used time of flight measurements in conjunction with a magnetic analyzer with nuclear emulsion detection. The electron beam

used in this work was of generally lower voltage and higher current than the Ion Physics beam. The observed ion energies at PI are lower than those at IPC, but the charge states are in agreement. In Reference 33 the PI investigators find that ion energy is increased by raising the electron energy and lowering the current which puts the two sets of data in closer agreement. The PI observation of ion energy being linearly dependent on charge state agrees with IPC data. The observation of multiple pulses and Rander's[28] finding of equal beam front and ion velocities is in contradiction to the IPC data. An explanation of some of the difference in results is offered by Putnam in another paper in these proceedings.

In conclusion, the handling of pulsed, relativistic, high current electron beams is in good shape technically. The theory, which was not discussed in this talk, has not yet had the effort put into it that the experimental work has. The application of these beams is still in its infancy.

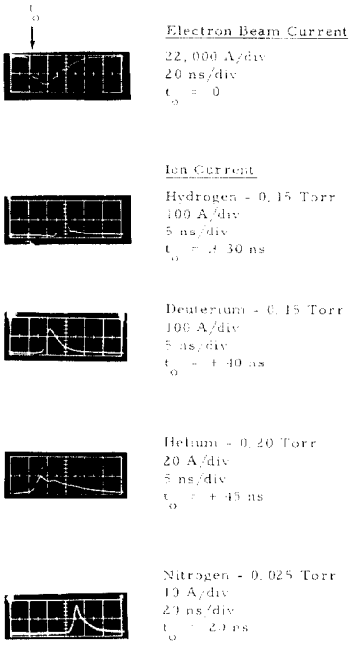

Figure 22. Representative ion pulses (carbon cathode)

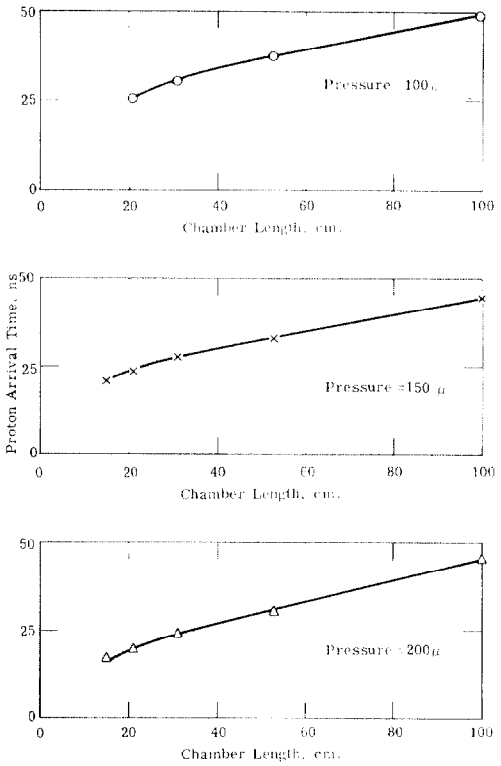

Figure 23. Proton arrival time versus drift tube length.

REFERENCES

1. W. H. Bennett, Phys. Rev. 45, 890 (1934); 98, 1584 (1955).
2. J. D. Lawson, J. Elec. and Cont. 3, 587 (1957); 5, 146, (1958).
3. H. Alfven, Phys. Rev. 55, 425 (1939).
4. J. C. Martin, Private Communication.
5. S. E. Graybill and S. V. Nablo, Appl. Phys. Letters 8, 18 (1966).
6. J. E. Rizzo, JAP 41, 4941 (1970).
7. W. T. Link, IEEE Trans. on Nuclear Sci. NS-14, 777 (1967).
8. S. E. Graybill and S. V. Nablo, IEEE Trans. on Nucl. Sci. NS-14, 782 (1967).
9. F. M. Charbonnier et al, IEEE Trans. on Nucl. Sci. NS-14, 782, (1967).
10. J. J. Clark, M. Ury, M. L. Andrews, D. A. Hammer, S. Linke, Record of the 10th Symposium on Electron, Ion and Laser Beam Technology, L. Marton, Ed. IEEE Catalog No. 69C22-ED, p. 117, (1969).
11. T. H. Martin, IEEE Trans. on Nuc. Sci. NS-16, p. 59, (1969).
12. G. Yonas, P. Spence, Record of the 10th Symposium on Electron, Ion and Laser Beam Technology, L. Marton, Ed. IEEE Catalog No. 69C22-Ed, p. 443, (1969).
13. J. R. Uglum, W. H. McNeill, S. E. Graybill, Record of the 10th Symposium on Electron, Ion and Laser Beam Technology, L. Marton, Ed. IEEE Catalog No. 69C22-ED, p. 155, (1969).
14. W. T. Oliphant, I. M. Vitkovitsky, Bull. Amer. Phys. Soc. 15, 1401, paper 1B8 (1970).

15. T. Martin, K. Prestwich, D. Johnson, Sandia Report SCRR-69-421 (1969).
16. J. D. Lawson, J. Nuc. Energy, Part C, Plasma Physics 1:31-35 (1959).
17. M. Andrews, J. Bzura, H. Fleischmann, N. Rostoker, Phys. of Fluids 13, 1322 (1970).
18. J. Bzura and S. Linke, Bull. APS 15, 1452 (1970) and Private Communication.
19. M. Friedman and M. Ury, Rev. of Sci. Instruments, 41, 1334 (1970).
20. J. Benford and B. Ecker, Bull. APS 15, 1401 (1970).
21. R. B. Oswald, F. B. McLean, D. Schallhorn, L. D. Buxton, Appl. Phys. Letters, 16, 24 (1970).
22. R. B. Oswald, D. R. Schallhorn, H. A. Eisen, F. B. McLean, Appl. Phys. Letters, 13, 279, (1968).
23. R. B. Oswald, Private Communication.
24. H. Fleischmann, Private Communication.
25. J. R. Uglum, S. E. Graybill, S. V. N blo, Rev. Sci. Instruments 40, 1413 (1969).
26. S. E. Graybill and J. R. Uglum, JAP 41, 236 (1970).
27. J. Rander, B. Ecker, G. Yonas, D. J. Drickey, Phys. Rev. Letters, 24, 283 (1970).
28. J. Rander, Phys. Rev. Letters, 25, 893 (1970).
29. S. Putnam, Phys. Rev. Letters, 25, 1129, (1970).
30. S. E. Graybill and J. R. Uglum, Bull. APS 14, 1048 (1969).
31. J. R. Uglum, S. E. Graybill and W. H. McNeill, Bull. APS 14, 1047 (1969).
32. N. Rostoker, Bull. APS 14, 1047 (1969).
33. J. Rander, B. Ecker, G. Yonas, Bull. APS 14, 1048 (1969) and Internal Report PIIR-9-70.
34. D. Hammer, F. Oliphant, I. Vitkovitsky and V. Fargo, Private Communication 1970. (To be published.)
35. J. E. Boers and D. Kelleher, JAP 40, 2409 (1969).